

Sam White?

att

0-5

NATIONAL AERONAUTICS AND SPACE ADMINISTRATION

High Explosives

TECHNICAL REPORT
R-23

EFFECT OF SURFACE ROUGHNESS ON CHARACTERISTICS OF SPHERICAL SHOCK WAVES

By PAUL W. HUBER and DONALD R. McFARLAND

*Index: (1) Explosion Effects, Shock Waves
(2) Blast Wave, Model Study
(3) Weapon Effects, Blast Wave
Model Study*

DISTRIBUTION STATEMENT A
Approved for Public Release
Distribution Unlimited

Reproduced From
Best Available Copy

1959

20011011 053

NASA/224

TECHNICAL REPORT R-23

**EFFECT OF SURFACE ROUGHNESS ON CHARACTERISTICS
OF SPHERICAL SHOCK WAVES**

By PAUL W. HUBER and DONALD R. McFARLAND

**Langley Research Center
Langley Field, Va.**

TECHNICAL REPORT R-23

EFFECT OF SURFACE ROUGHNESS ON CHARACTERISTICS OF SPHERICAL SHOCK WAVES ¹

By PAUL W. HUBER and DONALD R. MCFARLAND

SUMMARY

A small-scale laboratory investigation has been conducted in which direct observation of shock-wave movement with time was made and the effects of surface roughness on the characteristics of spherical shock waves were determined. Data were obtained with 15-gram pentolite charges at four heights of burst, both for a smooth surface and for a surface completely covered with pyramid-shaped roughness elements. The observations resulted in determinations of shock peak overpressure and Mach stem height as a function of distance for each test condition.

Comparison of the smooth-surface data with those obtained for the extremely rough condition showed a small reduction in the shock peak overpressures at the surface for all burst heights. The effect of extreme surface roughness on the Mach stem formation and growth was to delay the formation at the greatest charge height and to lower the height of the Mach stem for all heights of burst.

Comparison of the free-air shock peak overpressures with larger scale data showed good similarity of the overpressure-distance relationships. No geometrical similarity parameter was found which would describe the Mach stem growth in a manner independent of charge height, as suggested by other investigators; however, when the data were plotted in terms of a parameter relating the horizontal distance to the theoretical point of Mach stem formation, only a small influence of burst height on the path of the triple point was noted.

Although the data presented provide knowledge of the combined effect of many surface-roughness

elements on the overall shock characteristics, the data do not provide an insight into the details of the air-flow characteristics along the surface nor into the relative contribution of individual roughness elements to the results obtained.

INTRODUCTION

In studying the motion and properties of a shock wave moving along a surface, it is expedient to regard the surface as rigid and plane and the flow as nonviscous and nonheat-conducting. The problem is then reduced to one of wave reflection where the reflected wave properties are dependent only upon the relationship of the surface to the oncoming wave and to the incident wave strength, which are, in turn, space or time functions for spherical shocks. (For a comprehensive discussion of these shock reflections, see refs. 1 and 2.) When the surface is nonplanar, that is, with waviness, steps, or protuberances, the problem of the wave diffraction is not amenable to analytical solution. If the flow behind the shock is considered to be viscous, and if heat exchange can occur between the fluid and the surface, then the resulting energy and entropy changes in the fluid near the surface will produce some distortion and weakening of the shock wave, an effect which, for spherical shocks, is not possible to compute by means of existing theory. In the actual case of a large-scale blast over terrain which might include hills, trees, buildings, and so forth, it would be expected that wave diffraction, viscous flow, and heat conduction would occur near the surface. In addition to these effects, some

¹ Supersedes recently declassified NACA Research Memorandum L55B04 by Paul W. Huber and Donald R. McFarland, 1955.

cavitation of the surface, that is, erosion of surface material as well as refraction effects due to thermal gradients near the surface, might occur to complicate the conditions further. If the net result of these surface effects is to change the shock-wave strength and pattern, then recourse to actual observation of such phenomena would appear necessary for an understanding of the importance of surface effects in spherical shock-wave flows. Such observations would ideally include measurements of space-time distributions of pressure, fluid-flow velocity, temperature, and shock-reflection pattern, although measurements of one or two of these quantities would contribute much to a general understanding of the problem.

In reference 3, measurements of Mach stem heights of blast waves moving over smooth hard-packed dirt and smooth dry sand indicated that the path of the triple point in the case of dry sand was lower than that for hard-packed dirt. Although no explanation for this difference was available, it was speculated that, because of its porosity, the sand may act relatively more as an absorber, that is, less as a rigid reflector than dirt, and hence may weaken the reflected wave. It is also to be noted that higher ambient air temperatures existed for the dry-sand tests, which could indicate slightly weaker shock strengths. Possibly, in the case of dry sand some erosion of the sand also took place in the air flow behind the shock and resulted in energy extractions from the flow. In reference 4, measurements of Mach stem heights of blast waves passing over rows of solid walls located transversely to the wave on a smooth surface indicated that the formation of the Mach stem was delayed and the path of the triple point was lowered by the walls.

The results obtained in references 3 and 4 show, therefore, that some alteration of the wave pattern, at least locally, does occur because of differences in surface conditions. Delayed Mach stem formation and growth indicate that either the reflected wave strength has been reduced or that the wave has been distorted near the surface so that Mach stem formation is delayed. However, these effects may be only local, that is, near the surface, and may be manifested only when the shock is in the immediate vicinity of the perturbing factor.

The effect of patterned surface roughness on the overpressure characteristics of plane shock

waves was experimentally determined in a 4-by 7½-inch shock tube in reference 5. Attenuation of the shock-wave overpressure by as much as 30 percent was measured for a roughness size of ¼ inch. In this case of channel-type flow, however, any wave quantities generated near the surface as a result of viscous action must remain confined within the walls of the shock tube, and any such net effect must propagate along the axis of the shock tube. Since the shock-tube flow is usually many times longer than the cross-sectional dimension, the shock strength at all points across the channel is almost equally affected by all previous viscous surface action along the flow path. Reasonably, then, the magnitude of the attenuation in this quasi-one-dimensional type of flow can be expressed in terms of the surface-volume ratio of the shock tube (reciprocal of hydraulic radius in pipe flow).

In the case of a spherical shock wave moving over a surface, however, three-dimensionality of the pressure and flow patterns exists in the neighborhood of the surface with the result that concepts of wave attenuation established by the shock-tube tests are not applicable. For this reason, an investigation of the effects of surface roughness on spherical shock waves was made in the Gas Dynamics Branch of the Langley Laboratory by duplicating, as reasonably as practicable on a small scale, the actual shock-wave conditions.

The small scale of this investigation was chosen so as to allow the safe use of instrumentation and equipment under controlled laboratory conditions. It was felt that even if the selection of such a small scale resulted in some variance of the data from large-scale blast data, the comparison of rough- and smooth-surface data could still be made. In this investigation roughness-element heights of ¼ inch would be equivalent to about 23.5 feet for a charge of 20 kilotons of high explosive charge. In order to obtain the maximum effect of roughness and for simplicity in evaluation of the experimental results, complete coverage of the surface with roughness elements was chosen as the surface condition to be used.

SYMBOLS

<i>a</i>	velocity of sound, ft/sec
<i>d</i>	horizontal distance from charge, in. or ft
<i>h</i>	height above surface, in. or ft

p	pressure, lb/sq in. abs
r	radial distance to center of burst, ft
t	time, sec
t_d	duration of positive overpressure, sec
V	shock-propagation velocity, ft/sec
W	charge weight (including estimated charge in detonator), lb
α	angle between horizontal and tangent to incident shock wave at triple point, $\tan^{-1} \frac{d_y}{h_c - h_y}$, deg
γ	ratio of specific heats
ϕ	angle between horizontal and line connecting d_e and triple point, $\tan^{-1} \frac{h_y}{d_y - d_e}$, deg
Subscripts:	
o	standard atmosphere
1	ahead of shock
2	immediately behind shock
c	charge
e	theoretical limit of regular reflection; for example, $\alpha_e = \tan^{-1} \frac{d_e}{h_c}$
y	point of intersection of incident, reflected, and Mach shock waves (called triple point)

EXPERIMENTAL METHOD

At any instant of time, the velocity of propagation of a point on any wave can be expressed in terms of the fluid properties existing locally about that point. In the case of a shock wave, the velocity of propagation with respect to the fluid ahead, along an axis normal to the wave, is expressed in terms of the pressure ratio across the wave, the velocity of sound, and the specific-heat ratio of the fluid as

$$V = a_1 \left[\frac{\gamma - 1}{2\gamma} \left(\frac{\gamma + 1}{\gamma - 1} \frac{p_2}{p_1} + 1 \right) \right]^{1/2} \quad (1)$$

where the ratio γ of the fluid is assumed to be invariant with temperature.

In the case of a shock wave moving into a fluid which is stationary, equation (1) also represents the velocity of propagation of the shock wave with respect to an observer.

If the velocity of propagation, undisturbed pressure, specific-heat ratio, and sound velocity are known, the shock peak overpressure can be

expressed from equation (1) as

$$p_2 - p_1 = p_1 \left\{ \frac{2\gamma}{\gamma + 1} \left[\left(\frac{V}{a_1} \right)^2 - 1 \right] \right\} \quad (2)$$

Inasmuch as the undisturbed properties of the fluid are known and can be held constant during a controlled laboratory blast, the variation of shock peak overpressure with time readily results from measurements of the variation of shock-wave-propagation velocity with time. This velocity variation was obtained by graphically determining slopes from plots of shock-wave position with time. These data points were obtained directly from schlieren photographs of the wave taken at eight regular and accurately known time intervals for each blast. This equipment is referred to hereinafter as the NACA nine-channel spark and was developed at the Langley Laboratory by Joseph Burlock.

With schlieren photographs from the NACA nine-channel spark, the free-air shock peak overpressure, Mach stem shock peak overpressure along the surface, and Mach stem height could be obtained as a function of time and position. The regular reflected peak overpressures could not be obtained by using this method since the velocity of the reflection point along the surface, for the case of regular reflection, is not related to the reflected peak overpressure.

Pressure-time measurements at seven surface locations were also made for each blast at the highest charge location by using rapid-response flush-mounted gages. These data served as check points for the shock overpressures obtained by the velocity method and, in addition, provided measurements of the variation of pressure with time behind the shock wave so that the duration of positive overpressure could be determined.

APPARATUS AND PROCEDURE

A schematic diagram of the apparatus and instrumentation is shown in figure 1, and photographs of the apparatus are shown in figure 2.

The wave table shown in figures 1 and 2 is the area over which the charges were detonated and the wave characteristics experimentally determined. This table was fabricated from 2-inch boiler plate machined smooth and flat on the upper surface. The table was 12 feet square and was supported by four large I-beams imbedded in

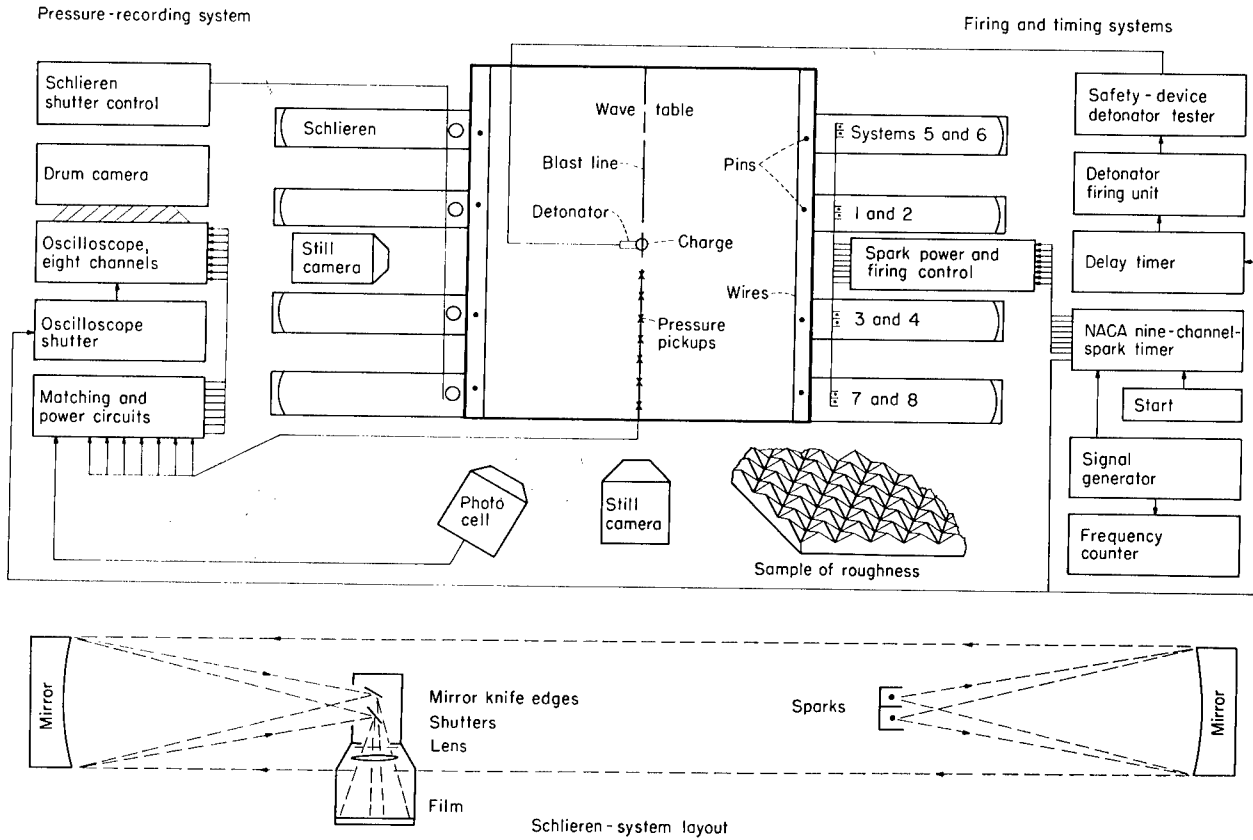


FIGURE 1.—Schematic diagram of wave table and instrumentation.



(a) With roughness.

(b) Support arm with 2-foot charge height.

FIGURE 2.—Views of wave table.

concrete so that the under surface of the table was accessible for mounting the pressure instrumentation and running electrical leads.

Roughness blocks were cast of 1-foot-square aluminum $\frac{1}{2}$ inch thick placed with the block edges parallel to the table edges to cover the upper surface of the table. The rough surface consisted of continuous rows of pyramid-shaped elements of $\frac{1}{4}$ -inch height and $\frac{1}{2}$ - by $\frac{1}{2}$ -inch base which were arranged to cover the surface of the block completely. These rows were orientated at an angle of 45° to the block edges and to the blast line. (See fig. 1.)

Directly over the center of the table and at any predetermined height, a $13\frac{1}{2}$ -gram spherical-cast bare 50/50 pentolite charge was detonated. This charge has a detonator well which was $\frac{5}{16}$ inch in diameter and $\frac{1}{10}$ inch deep. The charges were suspended from a support arm by placing the charge in a mesh net and then hanging the net to a hooked metal rod which could be raised and lowered in the support arm. (See fig. 2(b).) The support arm was located in a plane at the center of the table and perpendicular to the blast line and consisted of a crescent-shaped plate of $\frac{1}{2}$ -inch-thick steel, one end of which was bolted to the tabletop at a point 3 feet away from the blast line and the other end of which was $3\frac{1}{2}$ feet above the table. These distances were sufficient to prevent any reflected waves from the support arm from overtaking the shock as seen along the blast line during the time of observation. The pentolite charge was detonated by an instantaneous electric

blasting cap having a shaped charge. This cap was inserted $\frac{1}{10}$ inch into the detonator well of the pentolite charge. The axis of the cap was perpendicular to the blast line and parallel to the tabletop, and lead wires were run up and along the top of the support arm. This cap was estimated to contain a charge of explosive energy equivalent to something over 1 gram of pentolite.

A row of seven pressure pickups was located along the blast line as shown in figures 1 and 3. These pickups were flush-mounted capacitor-type frequency-modulated carriers and used diaphragms with natural frequencies of 10,000 to 30,000 cycles/sec. When roughness was used, the pickups were inserted in the roughness to one-third the pyramid height, and the tap drill for the pickup was drilled through the roughness block. (See fig. 3.) The seven gage outputs were simultaneously recorded on two synchronous-motor drum cameras which photographed two four-channel oscilloscopes. These pickups could be statically calibrated by mounting them in a calibration box and recording the oscilloscope traces for a series of static pressures. Calibration up to 14.7 lb/sq in. abs could be made with the pickups in position on the table by evacuating the inside of the gage. These pickups measure pressure within an accuracy of about 2 percent of the full-scale pressure range for each diaphragm used.

Eight schlieren optical systems were arranged, as shown in figures 1 and 3, so that movement of the shock wave along the blast line could be recorded photographically. Two complete optical

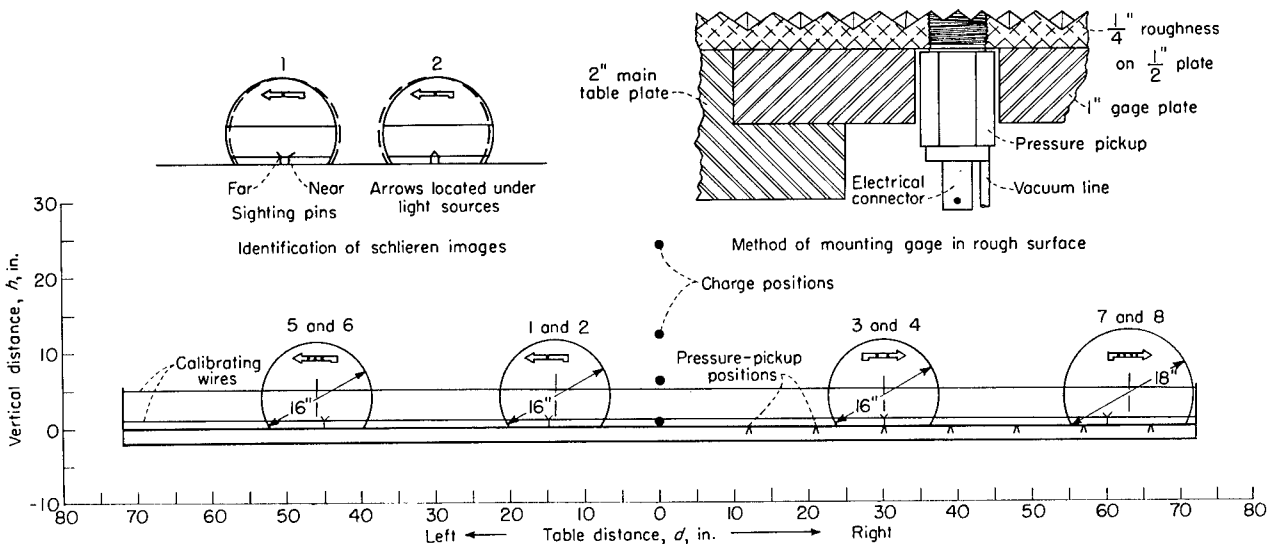


FIGURE 3.—Sectional view of table along blast line showing location of instrumentation.

systems were common to each pair of parabolic mirrors, and the mirror sets were placed along the blast line at increasing distances and alternately on opposite sides of the charge. In this manner, nearly complete coverage of an area including the 12 inches above the table surface and extending from a point 6 inches from the center of the table to the edge of the table along the blast line could be obtained optically.

The first three sets of mirrors had 16-inch diameters and 90-inch focal lengths, and the fourth set had an 18-inch diameter and a 105-inch focal length. Both the sources and knife edges were offset $\frac{3}{8}$ inch from the optical center of the system which produced an angularity of the light beam of less than $\frac{1}{4}^\circ$. One 5- by 7-inch camera focused on the blast line was used to record the images of each pair of optical systems.

The eight high-voltage sparks used for light sources of the schlieren systems were electronically controlled to fire at any predetermined firing rate by means of the NACA nine-channel spark. This timer consisted of an electronic ring counter controlled by a signal generator so that the ring counter would produce a spiked pulse at a precise point of each signal cycle in successive channels of the timer. Each pulse would then fire a high-voltage thyratron located in one of the eight high-voltage power supplies to the sparks. The ionization time of the spark sources was held at a minimum by means of radioactive paint on the electrodes. The response of the NACA nine-channel spark and spark source to a given signal input is believed to be consistent within a few microseconds.

The first of the nine pulses was used to initiate an interval-delay timer which controlled the firing circuit for the detonator so that the remaining eight pulses would be synchronized with the shock movement along the table. This initial pulse also controlled the electronic shutter of the oscilloscopes so that the pressure-gage traces would be recorded for a period of 1 revolution of the drum cameras. Also recorded on the drum cameras in the earlier tests was the trace from a photomultiplier tube which was mounted to face the fireball. Two 5- by 7-inch still cameras were placed so as to record a time-integrated photograph of the fireball from two views 90° apart.

In order to obtain accurate measurements of shock position from the schlieren photographs and

for convenience in adjustment of the optics and identification of the film, four small steel pins and two tightly stretched piano wires were located along each of the two edges of the table parallel to the blast line as shown in figures 1 and 3. These pins and wires appear in the schlieren photographs and provide a reference point and length scale for each record. Because of the slight angularity of the schlieren light beams, the pair of steel pins common to each system would not appear superimposed on the film; thus, in order to obtain a reference point on the blast line, it is necessary to take a point halfway between the images of the pins. The tops of the pins were bent so that the schlieren photograph showing the pins bent away from each other was the earlier of the two photographs in each set as shown by the insert in figure 3. A frequency counter was used to read the frequency of the signal generator and could be stopped immediately after a detonation. The stability of the signal generator and accuracy of the counter were such that the frequency was known to about 1 part in 1,200.

Insofar as was possible, the electronic equipment and instrumentation were located in a control house constructed about 15 feet away from the wave table. It was necessary, however, for the optical systems and high-voltage equipment to be located near the table, and in these cases plywood shielding was used to protect against copper fragments from the detonator caps and to provide for light shielding from the fireball. The cameras were also shielded against reflected light from the room, and solenoid-operated camera shutters were located directly behind the knife edges.

Preliminary to each series of detonations, the charge to be used was weighed to the nearest 0.01 gram with a chemical balance. Then, the pressure gages were calibrated statically by both of the methods mentioned previously at a series of pressures which would cover the pressure range of each gage. Immediately before the detonation one calibration pressure trace for each gage using the evacuation method was superimposed on the drum-camera record.

The pentolite charge was suspended over the center of the table by means of a plumb line, and the height of charge was measured with a scale to the nearest $\frac{1}{2}$ inch. (See fig. 2(b).) When roughness was used, the height of charge was measured from a point at one-third the pyramid height, the

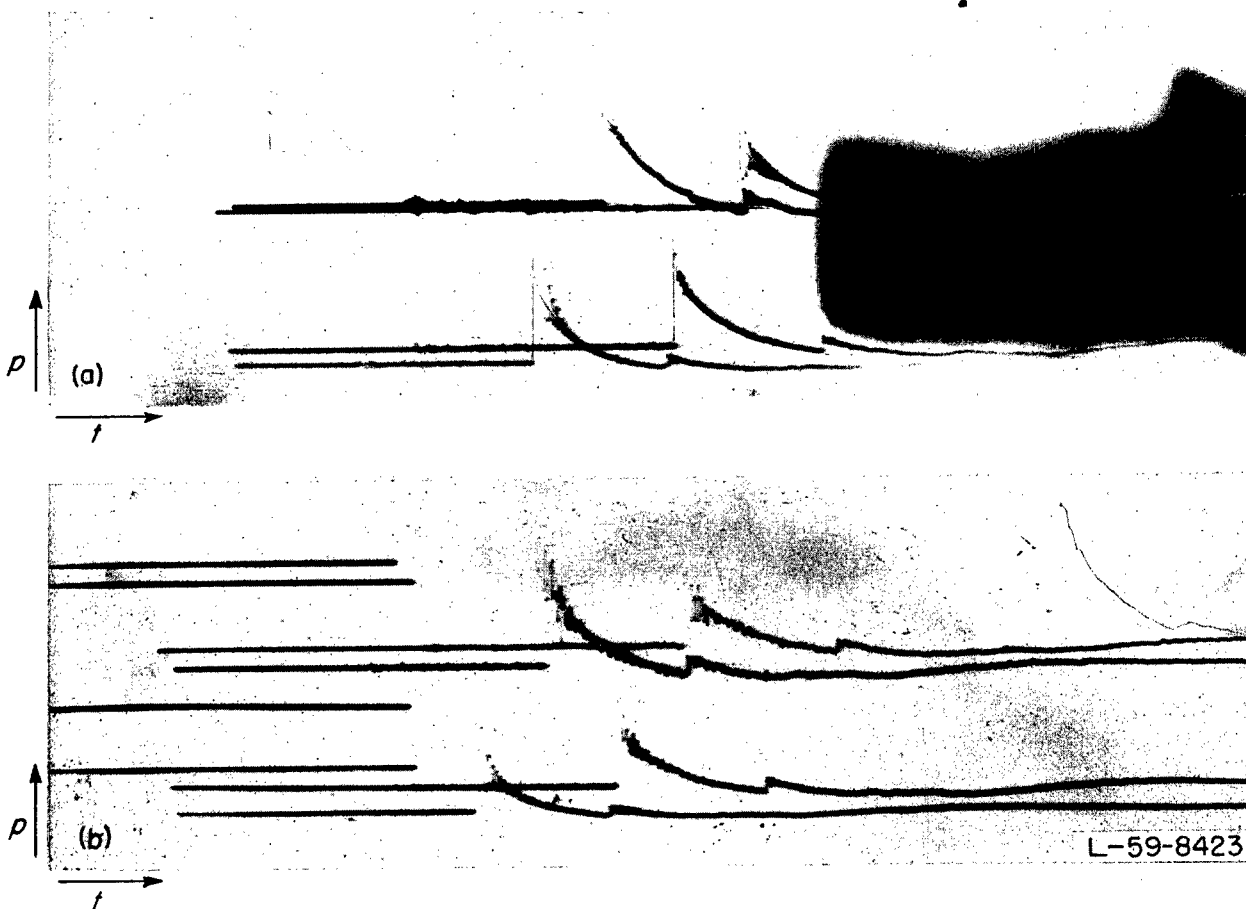
justification being that this would be the location of a smooth surface of equal displacement.

Immediately prior to a detonation the signal generator was set to the desired frequency and the delay of the firing circuit was set to the desired value. The temperature and pressure in the laboratory were recorded, and all fans and ventilators were shut off. The drum cameras were started, the room lights were shut off, and the shutters of the schlieren and still cameras were opened. Immediately after the detonation the signal-generator frequency was recorded.

Data were read from the drum-camera and schlieren films by means of a comparator. The accuracy of measurement of the films was better than 0.01 inch with this method. The peak-over-pressure readings from the drum-camera records were obtained by fairing through the mean values of the gage-ringing oscillations. (See figs. 4(a) and 4(b).)

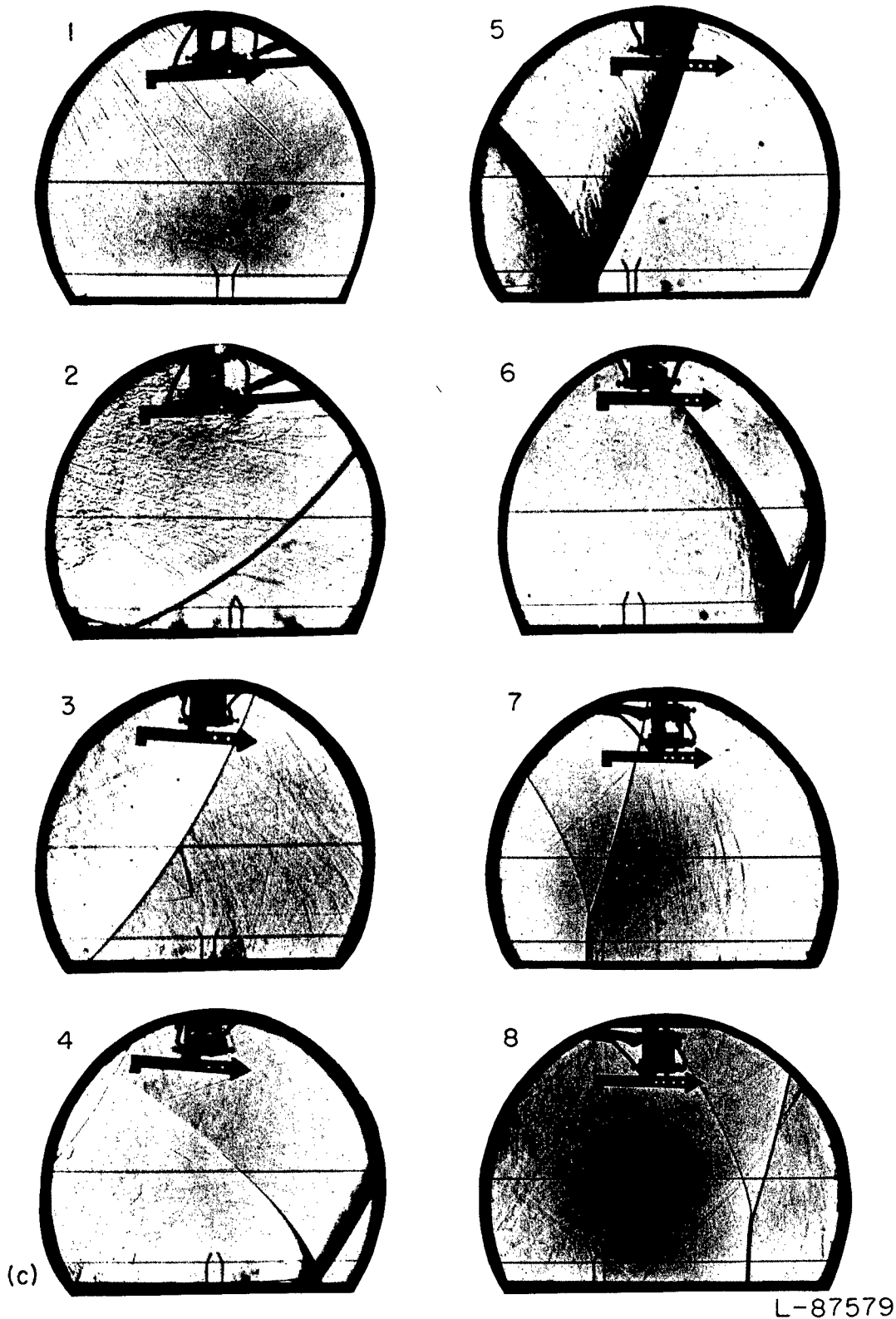
PRESENTATION OF RESULTS

A typical set of schlieren photographs showing the shock-wave movement along the smooth surface is shown in figure 4(c) and along the rough surface in figure 4(d) for a charge height of 2 feet. It is to be remembered that each of these figures (figs. 4(c) and 4(d)) represents photographs of a complete sequence for one particular burst. The photographs taken on the left side of the table are shown in a reversed direction so as to show all the waves moving from left to right. Various selected photographs (not of a particular sequence) showing some representative wave configurations are presented for a 1-foot charge height in figure 4(e) and for 6-inch and 0.5-inch charge heights in figures 4(f) and 4(g), respectively. This is believed to be the first direct systematic observation of Mach stem growth for spherical shock waves.



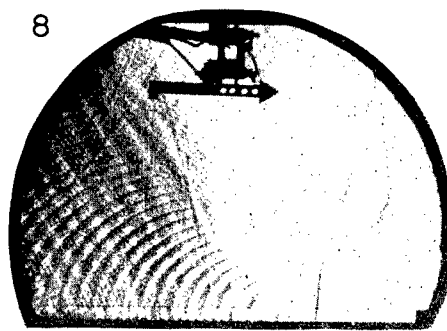
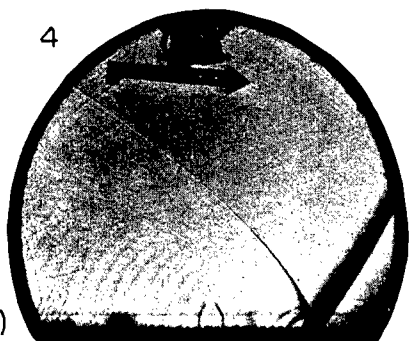
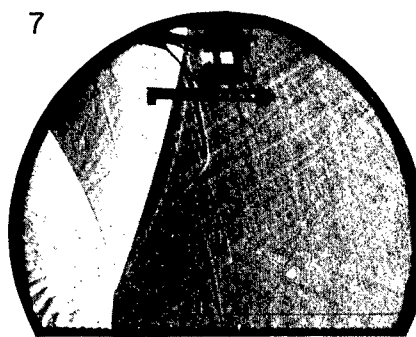
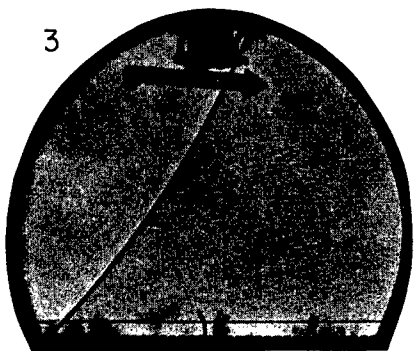
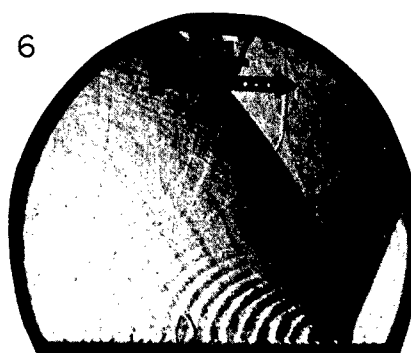
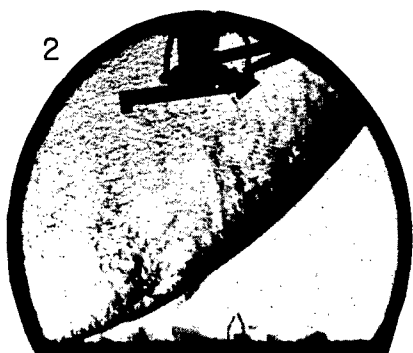
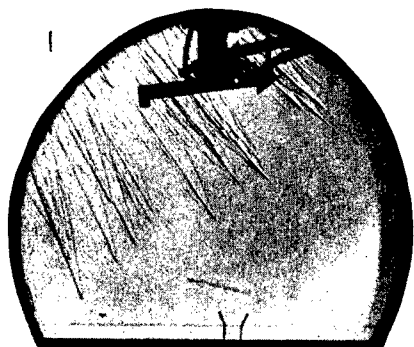
(a) Drum-camera pressure records for smooth surface for a 2-foot charge height.
 (b) Drum-camera pressure records for rough surface for a 2-foot charge height.

FIGURE 4.—Typical data records.



(c) Nine-channel schlieren photographs for smooth surface for a 2-foot charge height.

FIGURE 4.—Continued.

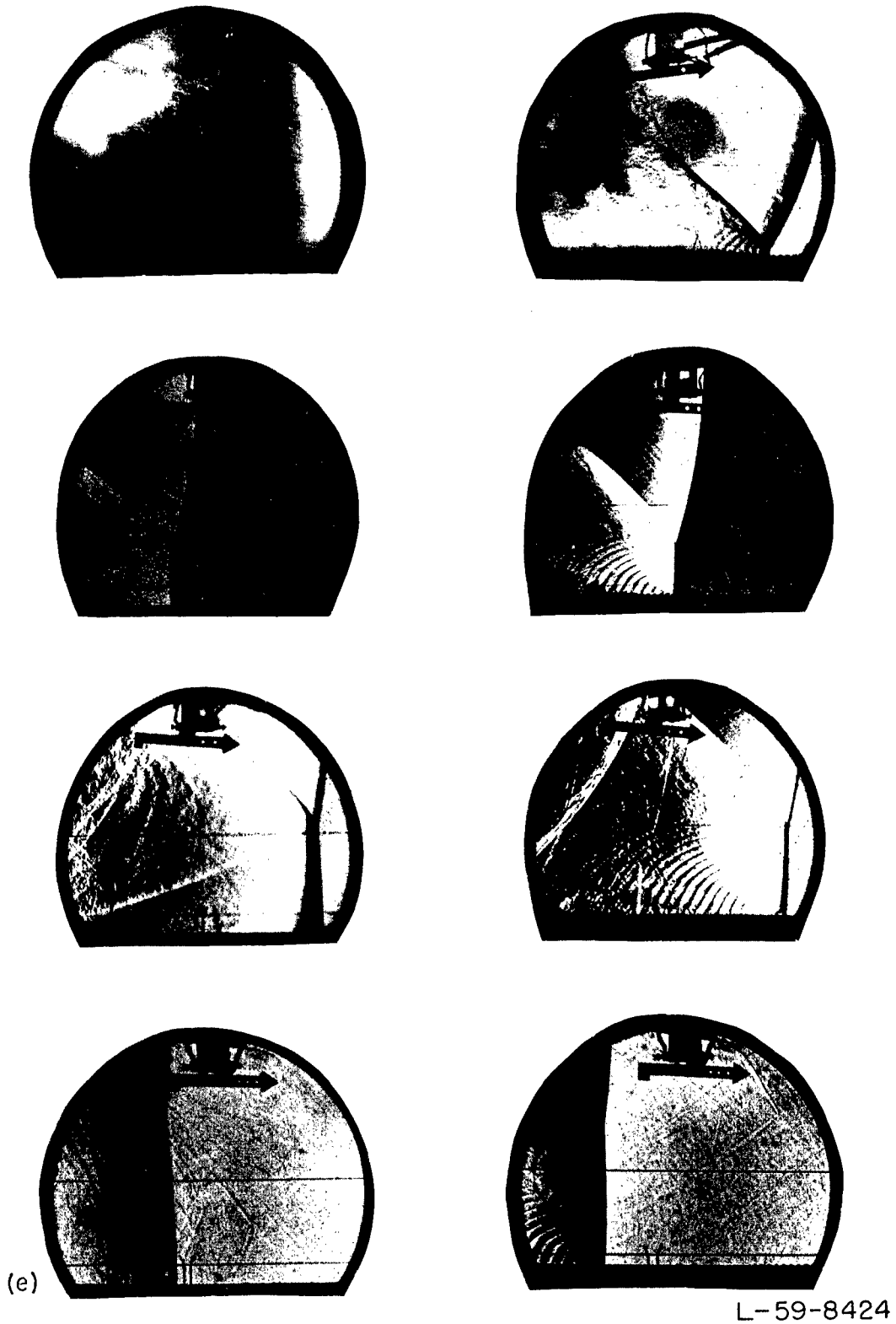


(d)

L-87580

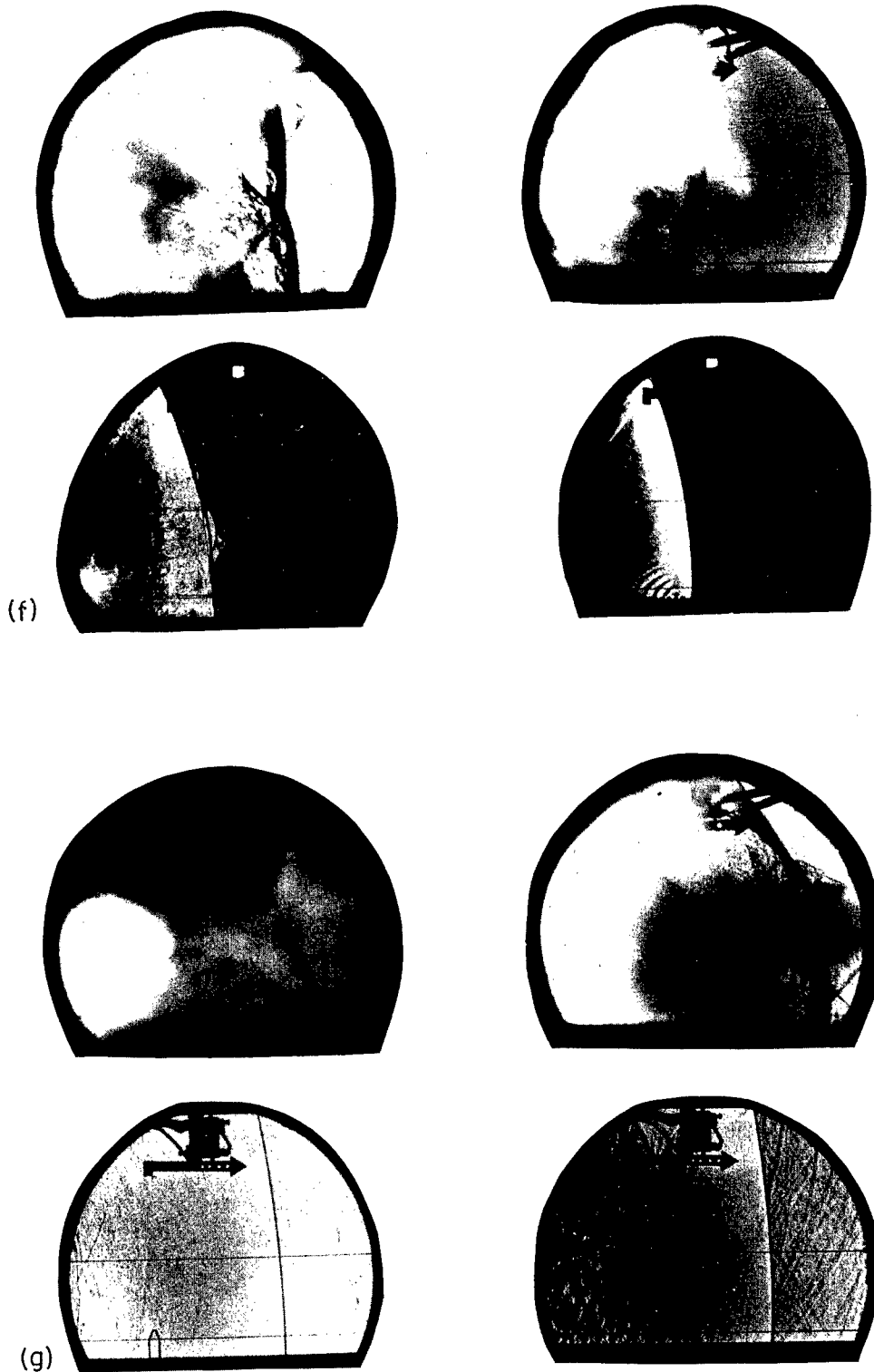
(d) Nine-channel schlieren photographs for rough surface for a 2-foot charge height.

FIGURE 4.—Continued.



(e) Selected schlieren photographs for both a smooth and rough surface for a 1-foot charge height.

FIGURE 4.—Continued.



(f)

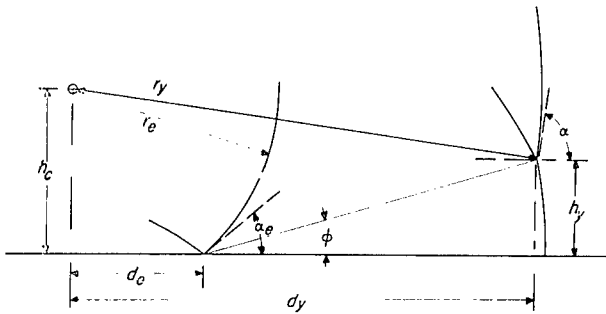
(g)

L-59-8425

(f) Selected schlieren photographs for both a smooth and rough surface for a 6-inch charge height.
(g) Selected schlieren photographs for both a smooth and rough surface for a 0.5-inch charge height.

FIGURE 4.—Concluded.

Typical pressure records are shown in figures 4(a) and 4(b) for both smooth-surface and rough-surface detonation, respectively, for a charge height of 2 feet. The geometrical relationship of the pertinent parameters as used to describe the wave configuration and as applied to the reading of the photographs is shown in sketch (a):



Sketch (a).

SHOCK STRENGTH

A typical time-distance history of the shock movement along the surface of the table and in free air taken from figure 4(c) is plotted in figure 5. The surface distance was measured horizontally from the center of the table to the point of intersection of the blast with the surface. The free-air distance was measured radially from the center of the charge to any convenient point on the incident shock wave, but not directly at the triple point. In both cases, the measurements were made at the extreme forward edge of the shock front. Selection of a more rearward point on the shock front would be doubtful because of possible refraction effects of the light passing through the wave.

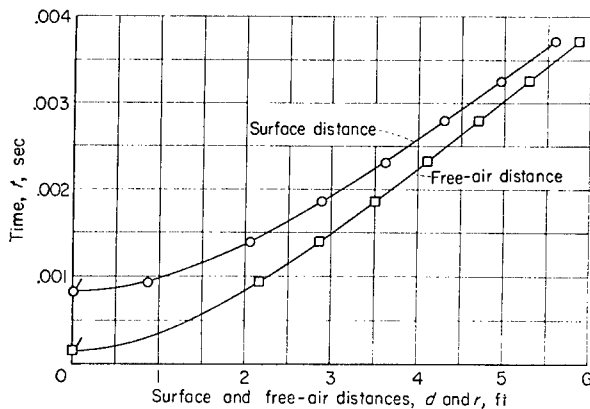


FIGURE 5.—Typical time-distance history of shock-wave movement along surface and in free air taken from figure 4(c). Flags indicate estimated data.

The values of time which are plotted are taken from the frequency-counter readings and start from the time that the first pulse of the NACA nine-channel spark is fired. As is the case in figures 4(c) and 4(d), the wave was seldom in the field of view in the first schlieren photograph with the result that only seven experimental points could be plotted for each curve. The time at zero free-air distance, which corresponds to firing the charge, is obtained from the photocell record and includes the interval-delay timer and the delay of the detonator. This point is plotted to aid in the fairing of the free-air curve. The delay of the detonator was kept almost constant in these tests (about 50 microseconds) by using a high-voltage-discharge firing circuit. The time point shown for zero surface distance was estimated and plotted to aid in fairing the surface-distance curve. This point was obtained by finding the free-air shock-wave velocity corresponding to the average of the distance from the charge to the table center and of the radial distance from the charge to the first visible incident shock wave, from accepted free-air data (ref. 6), and then by subtracting the resulting calculated travel time between these points from the first data point.

Slopes of the faired curves were then graphically obtained at each experimental data point on the plots, and the free-air shock peak overpressures obtained by this method using equation (2) are plotted in figure 6 for some typical tests. The overpressures are corrected to standard atmospheric pressure, and the distances are corrected to atmospheric pressure and are reduced to 1 pound of pentolite, according to the usual scaling laws for blast data, by using the combined weight of cap and charge as follows (see ref. 2):

$$(p_2 - p_1)_o = (p_2 - p_1) \frac{p_o}{p_1} \quad (3)$$

$$r_o = \frac{r}{W^{1/3}} \left(\frac{p_1}{p_o} \right)^{1/3} \quad (4)$$

Figure 6 shows that, although there is some scatter of the data, the results generally agree very well with larger scale data such as the data in reference 6. This fact would indicate that reducing the scale of the detonation to a much lower value than that used in previous shock-wave studies did not adversely affect the similarity of the blast pattern, which might be a little surprising

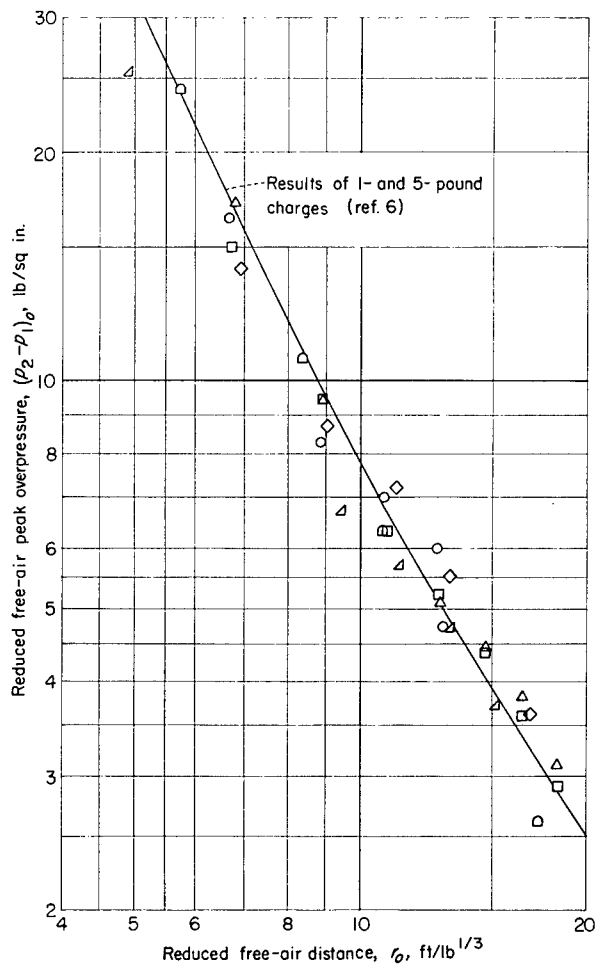


FIGURE 6.—Free-air pressures obtained from schlieren data. Each type of symbol represents a separate test.

in view of the relatively large ratio of cap size to charge size required for this work. Preliminary tests made with an electric cap small enough to be inserted completely into the charge showed a very poor reproducibility of the pressures with the result that the larger cap was actually necessary to obtain a true detonation consistently. The time-integrated images of the fireballs obtained with the still cameras qualitatively verified this fact by showing a more nearly reproducible light pattern with the larger cap.

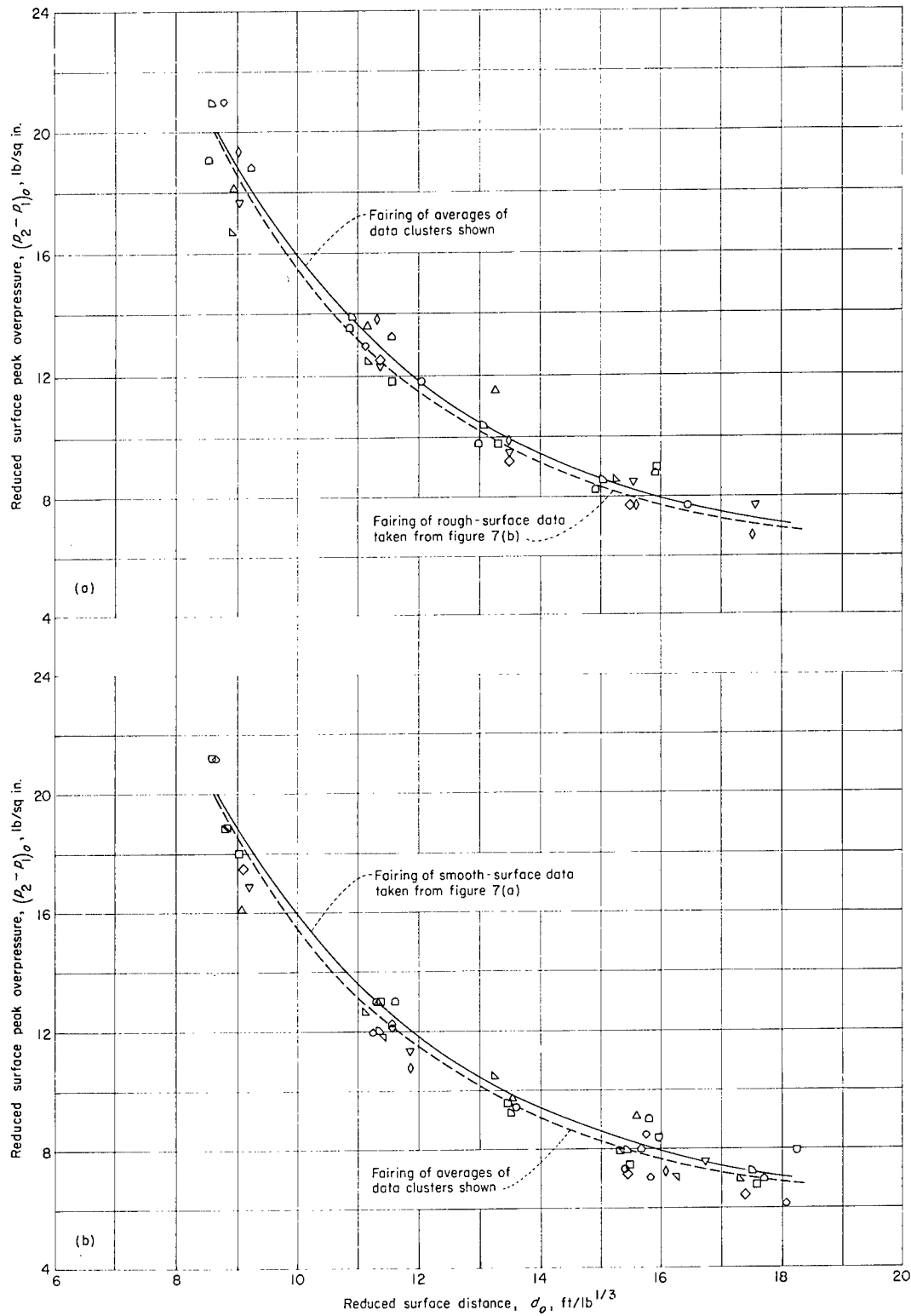
Mach shock peak overpressures along the surface were measured by this method for heights of burst of 2 feet, 1 foot, 6 inches, and 0.5 inch (reduced heights of 6.25, 3.125, 1.56, and 0.13 ft/lb^{1/3}) for both the smooth- and rough-surface conditions. These overpressures are plotted in

figures 7 to 10, respectively, and are reduced to standard atmospheric pressure and 1 pound of pentolite charge.

It can be seen from the fairing of the data-cluster arithmetic averages in figures 7 to 10 that, at all the heights of burst shown, a slightly lower Mach shock peak overpressure is obtained for the rough-surface condition. The magnitude of this difference, however, is less than the scatter of the individual data points and would not be easily distinguishable before averaging the data.

A plot of the peak overpressure along the surface as measured from the pressure-gage records is shown in figure 11 for a reduced height of burst of 6.25 ft/lb^{1/3} for both the smooth and rough surfaces. The faired curves taken from figure 7 are shown to aid in the comparison of the pressure-pickup results with the NACA nine-channel-spark data. The comparison is not particularly good, and the inconsistency in the pressure-pickup data is felt to be due mainly to uncertainty in interpreting the pressure record. A considerable amount of high-frequency oscillation of the pressure trace (gage-diaphragm "ringing" excited by the shock) was present and, at the higher values of shock overpressure, was of a magnitude equal to or greater than the shock peak overpressure. Since damping of this oscillation required about ½ millisecond, or 50 percent of the positive-overpressure duration, and since the trace became very light at this high "writing" speed, the film reading was uncertain in this region. Basically, of course, this inability to obtain accurate pressure-pickup data must be attributed to the small scale of the experiment inasmuch as the same damping time in relation to longer positive-overpressure durations would be less troublesome. Because of this difficulty and because it was felt that the NACA nine-channel-spark data are inherently more precise than pressure-pickup data, development of the pressure-pickup system was not pursued further.

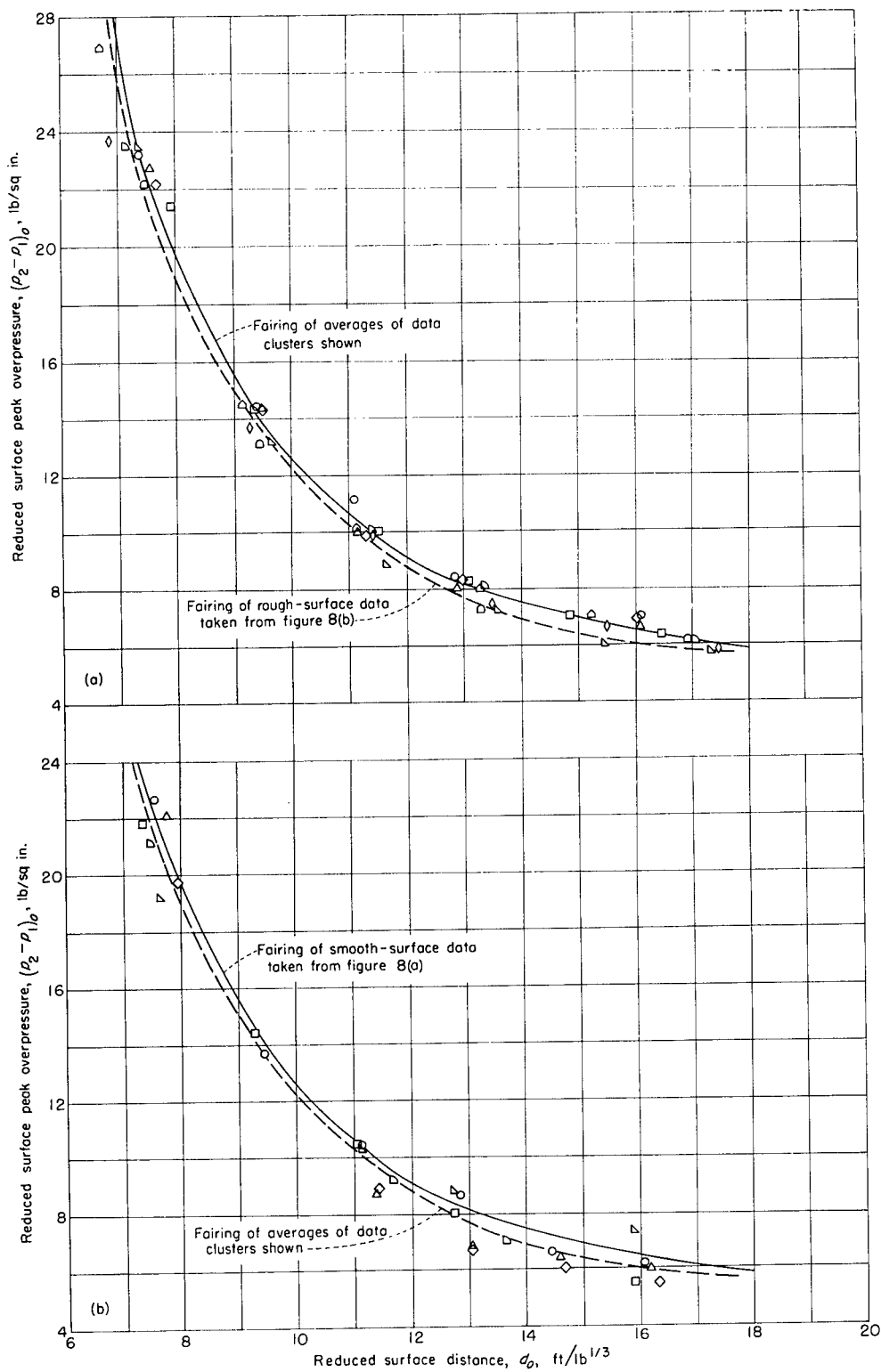
The duration of the positive overpressure was obtained from each pressure record, and the averages of these measurements are plotted in figure 12 for the reduced height of burst of 6.25 ft/lb^{1/3}. (Smooth-surface pressure data were not available for the three smallest distances.) Only slight differences in duration of the positive overpressure between the smooth- and rough-surface data are shown in figure 12.



(a) Smooth-surface data.

(b) Rough-surface data.

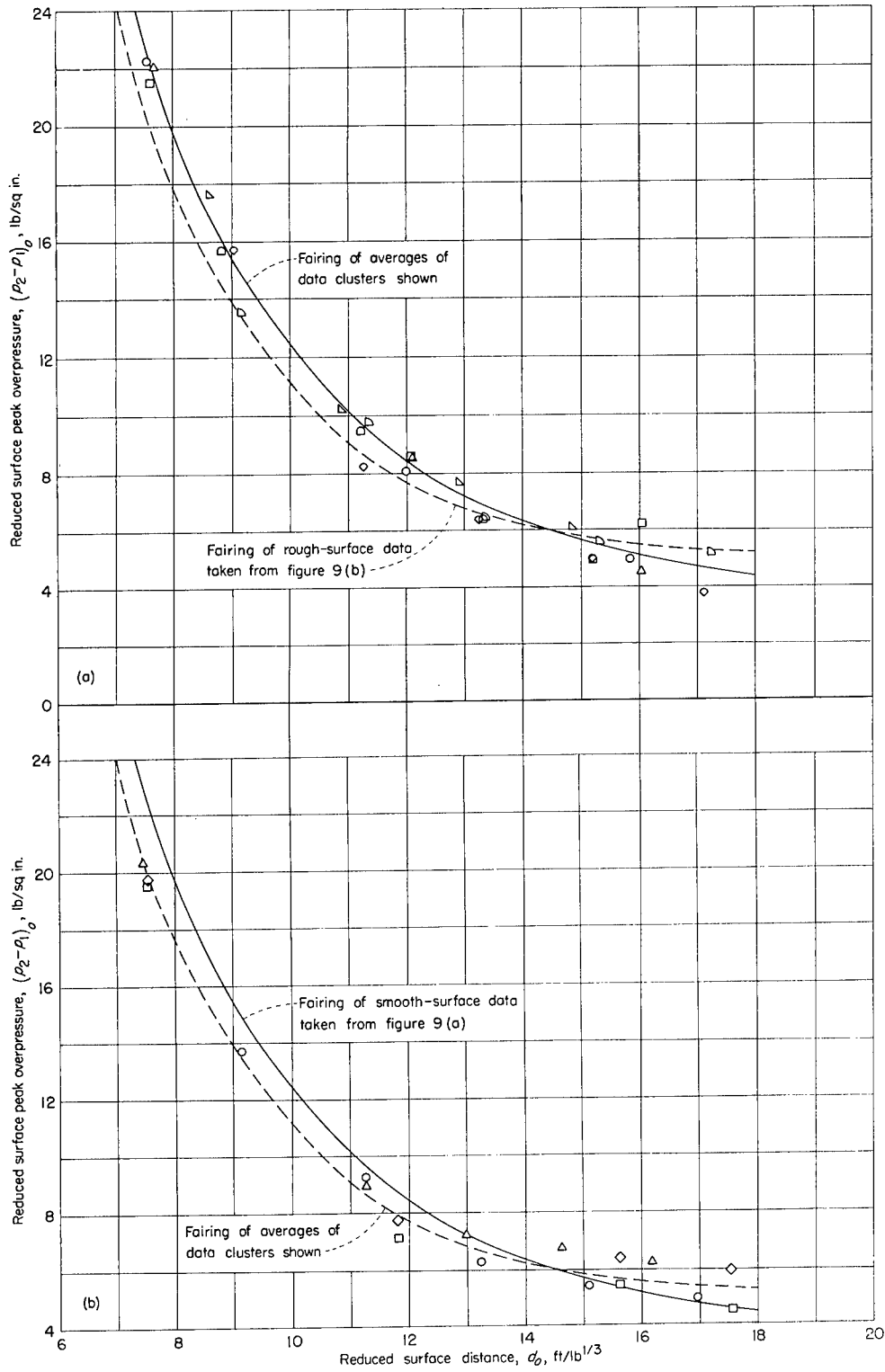
FIGURE 7 — Surface peak overpressures obtained from schlieren data for a reduced height of burst of 6.25 ft/lb^{1/3} (2-foot actual charge height). Each type of symbol represents a separate test.



(a) Smooth-surface data.

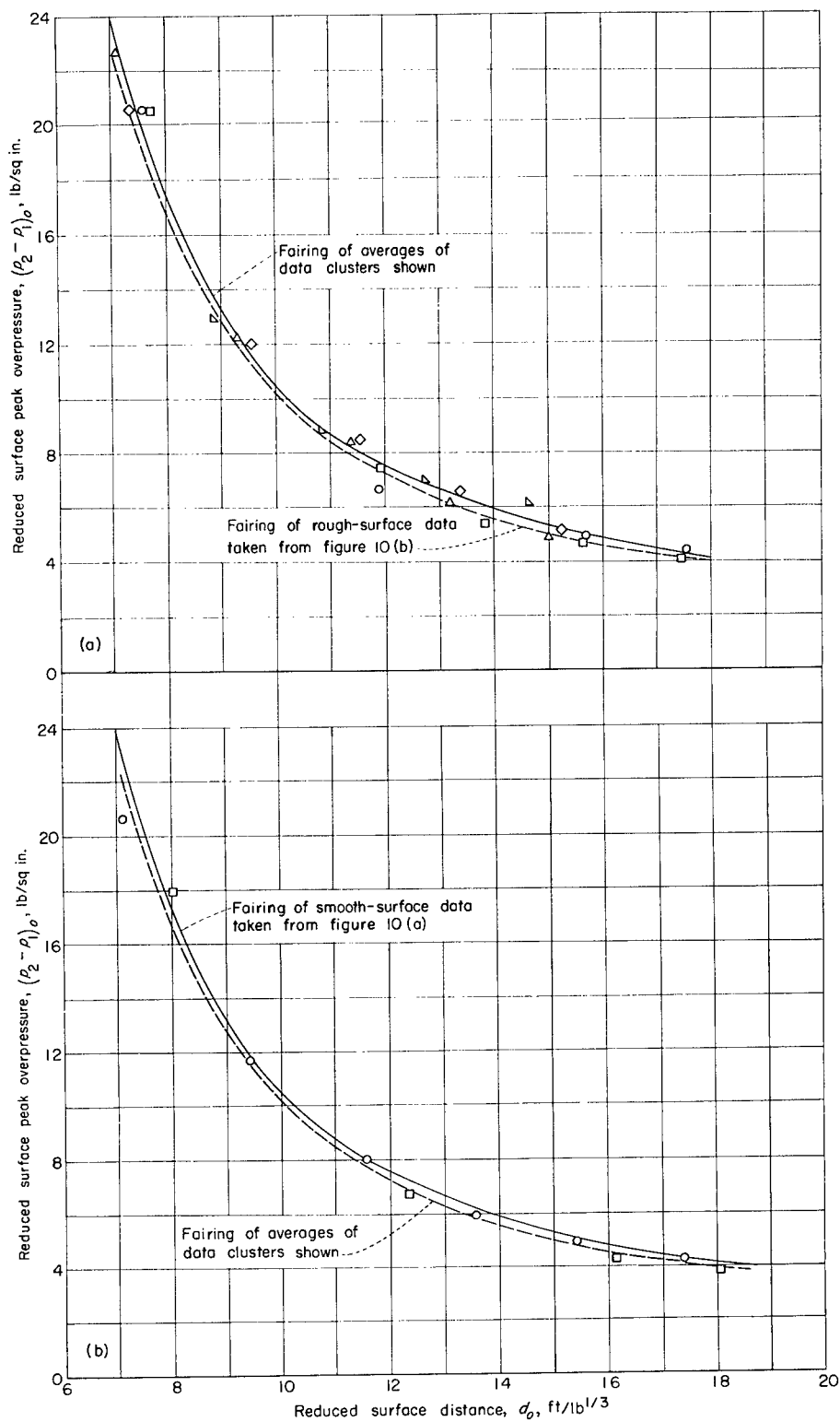
(b) Rough-surface data.

FIGURE 8.—Surface peak overpressures obtained from schlieren data for a reduced height of burst of 3.125 ft/lb^{1/3} (1-foot actual charge height). Each type of symbol represents a separate test.



(a) Smooth-surface data.
 (b) Rough-surface data.

FIGURE 9.—Surface peak overpressures obtained from schlieren data for a reduced height of burst of 1.56 ft/lb^{1/3} (6-inch actual charge height). Each type of symbol represents a separate test.



(a) Smooth-surface data.

(b) Rough-surface data.

FIGURE 10.—Surface peak overpressures obtained from schlieren data for a reduced height of burst of 0.13 ft/lb^{1/3} (0.5-inch actual charge height). Each type of symbol represents a separate test.

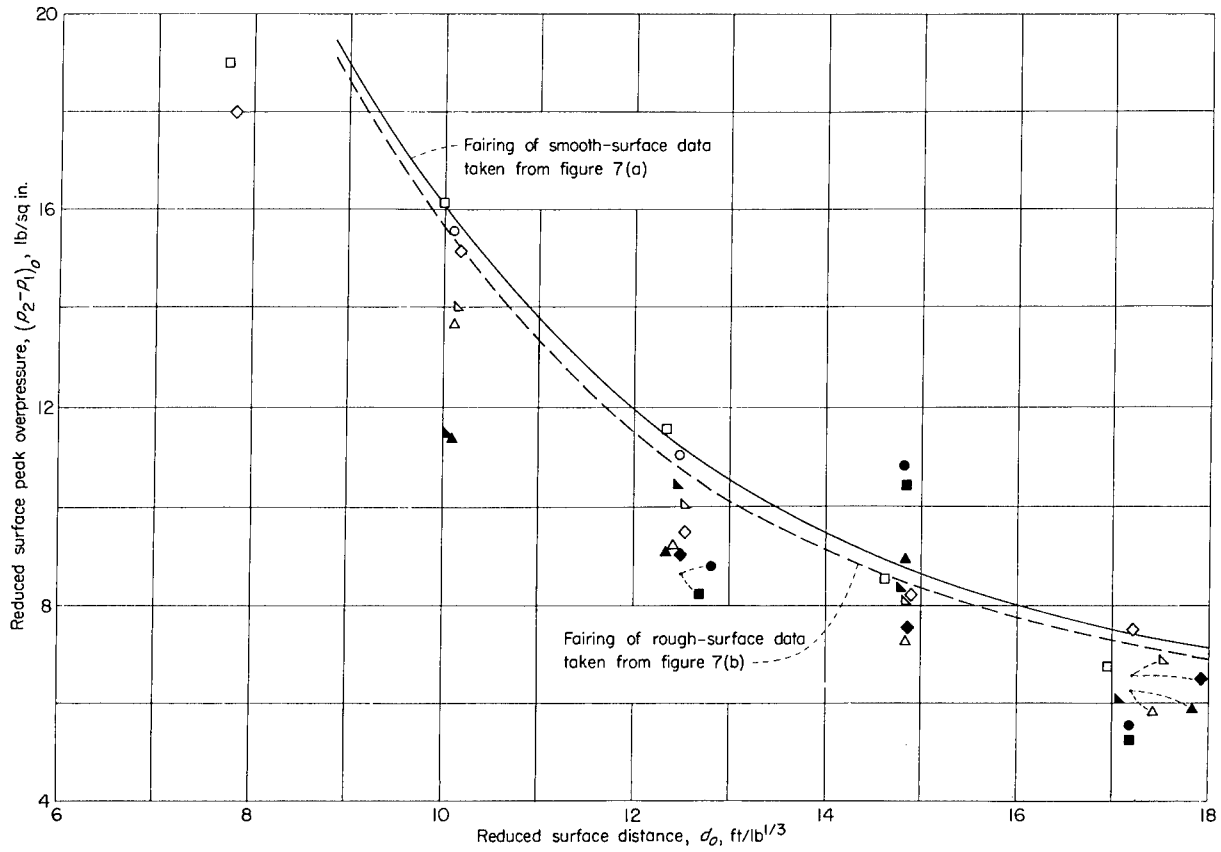


FIGURE 11.—Comparison of surface peak overpressures obtained from pressure pickups and fairing of schlieren data for a reduced height of burst of $6.25 \text{ ft/lb}^{1/3}$. Solid symbols represent smooth-surface data; open symbols represent rough-surface data; each type of symbol represents a separate test.

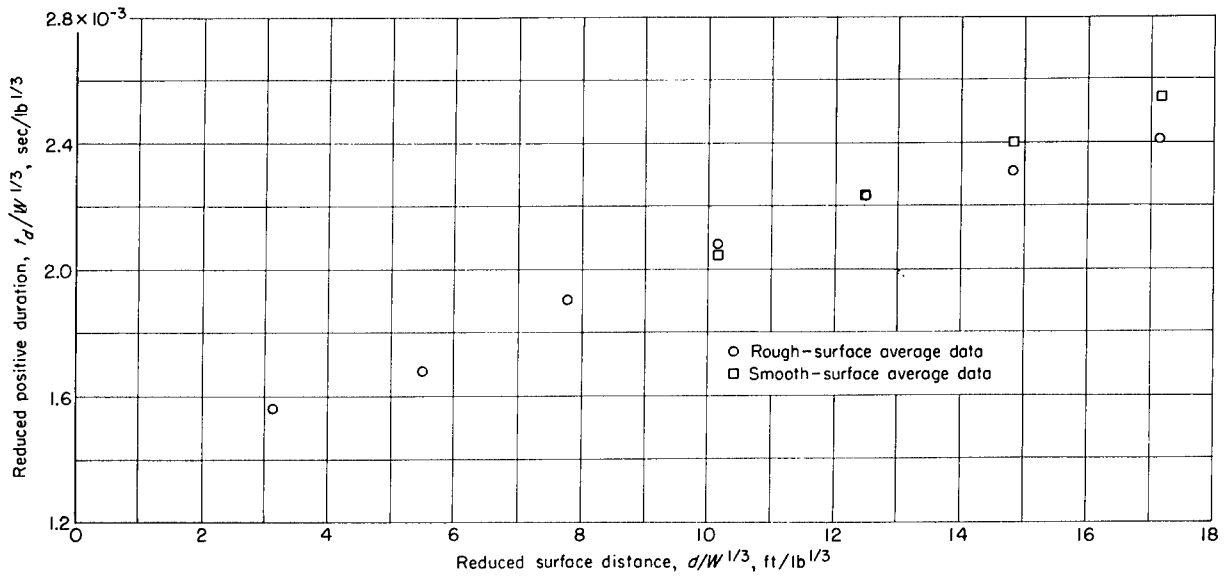


FIGURE 12.—Comparison of duration of positive overpressures of smooth- and rough-surface data for the reduced height of burst of $6.25 \text{ ft/lb}^{1/3}$. Data are not reduced to standard atmospheric conditions.

By using the data from the NACA nine-channel-spark peak-overpressure measurements, the height-of-burst curves are plotted in figure 13 for both smooth- and rough-surface conditions and are reduced to standard atmospheric pressure and 1 pound of pentolite charge. The data points shown are values taken from the faired curves in figures 7 to 10, and the solid and dashed curves in figure 13 are arbitrary fairings of these points for the smooth and rough surfaces, respectively. In figure 14 is shown a comparison of the height-of-burst curves of figure 13 with data points taken from reference 7. As was the case in figures 7 to 10, the differences in the smooth- and rough-surface data lie within the scatter of the individual data points taken from reference 7.

MACH STEM

Measurements of the Mach stem heights were taken directly from the schlieren photographs and are plotted for both the smooth- and rough-surface conditions and for reduced heights of burst of 6.25, 3.125, and 1.56 ft/lb^{1/3} in figures 15, 16, and 17, respectively. The arrows in these figures show

the theoretical points of Mach stem formation. (See ref. 1.) The curves drawn represent a fairing of the arithmetic averages of the data-point clusters for each surface condition. It can be seen from these figures that the Mach stem height is lower for the rough-surface condition at all three heights of burst shown and that the magnitude of the difference is, in general, greater than the scatter of the individual data points. These figures also show that the point at which the Mach stem begins to rise is delayed in the case of roughness at the greatest burst height and possibly at all three heights of burst. In order to present these data in a form which is more readily extrapolated, the faired curves and data-point averages of figures 15 to 17 are shown in logarithmic coordinates in figure 18. It appears from this figure that not only is the point of Mach stem formation possibly delayed for the rough condition at all heights of burst but the point of rise for the case of the smooth surface and the reduced height of burst of 6.25 ft/lb^{1/3} might also be delayed with respect to the theoretical rise point.

The faired data of figures 15 to 17 are compared with Mach stem measurements from references 3, 4, 8, 9, and 10 in figure 19. Figure 19 shows that the difference in measurements of Mach stem height for the smooth- and rough-surface conditions reported herein is less than the scatter of the

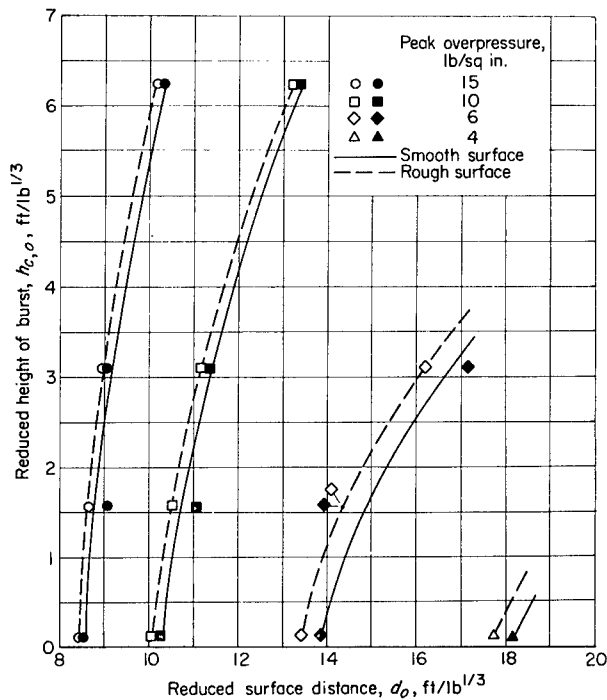


FIGURE 13.—Comparison of effect of height of burst on peak overpressure over smooth and rough surfaces. Solid and open symbols represent points taken from faired curves of smooth- and rough-surface data, respectively, of figures 7 to 10.

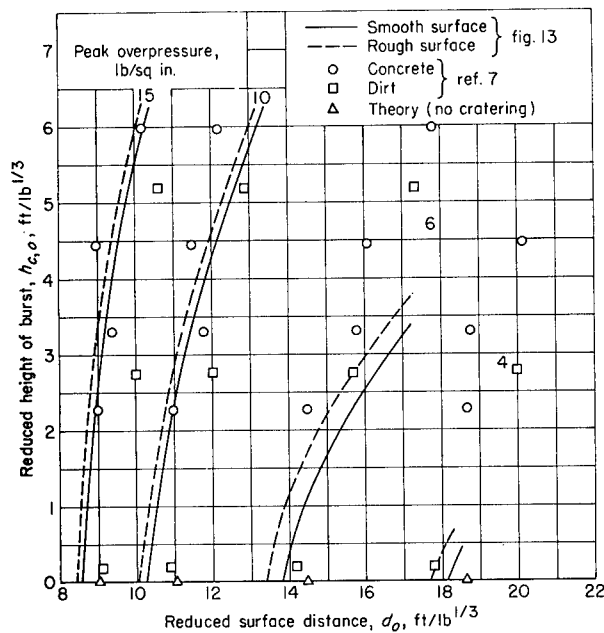


FIGURE 14.—Comparison of height-of-burst curves of smooth and rough surfaces with reference data.

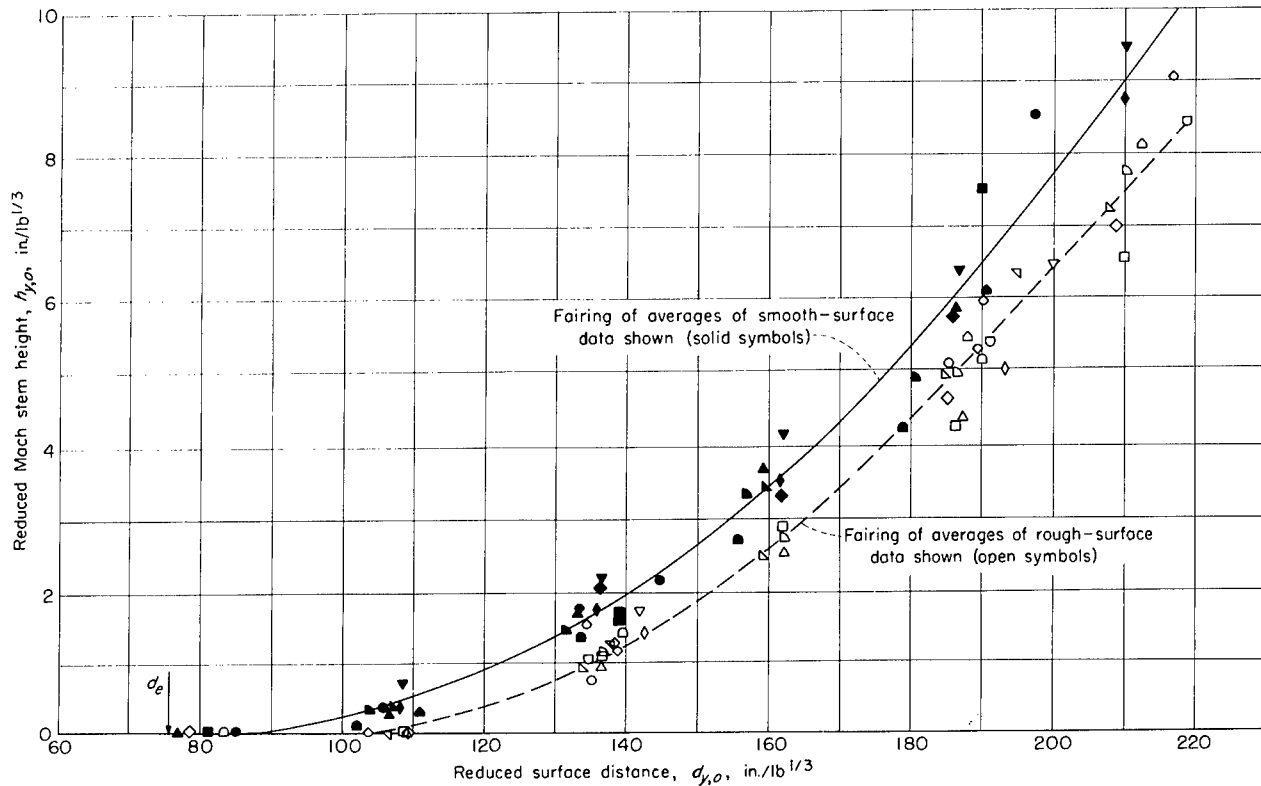


FIGURE 15.—Comparison of Mach stem growth over smooth and rough surfaces for a reduced height of burst of 6.25 ft/lb^{1/3}. Each type of symbol represents a separate test.

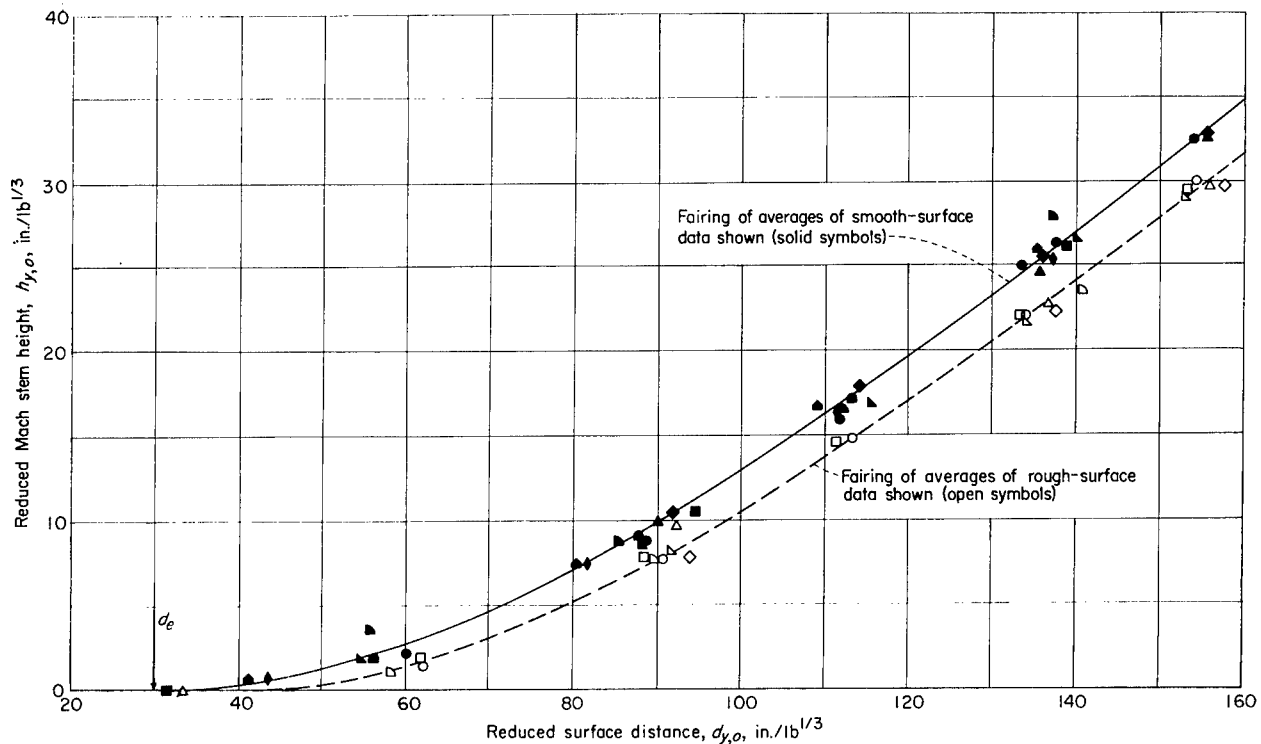


FIGURE 16.—Comparison of Mach stem growth over smooth and rough surfaces for a reduced height of burst of 3.125 ft/lb^{1/3}. Each type of symbol represents a separate test.

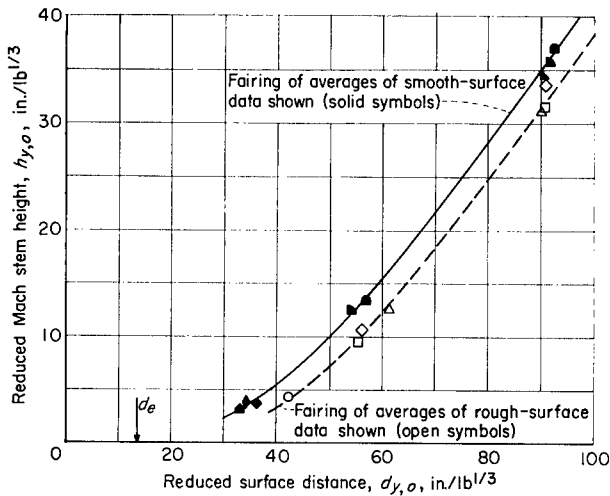


FIGURE 17.—Comparison of Mach stem growth over smooth and rough surfaces for a reduced height of burst of 1.56 ft/lb^{1/3}. Each type of symbol represents a separate test.

reference data. Since the reference data were obtained from surfaces not greatly different (with the exception of ref. 4) in comparison with the difference of surface conditions reported herein, it would not seem that the scatter of the reference data was due solely to surface conditions. It is to be noted that there is a basic difference, however, in the method used to obtain Mach stem height in this investigation from that used in the references. Although the measurements obtained herein are the result of direct observation of the shock intersections, the method used previously involved extrapolation of gage-height data against time-interval data to a zero-time interval in order to obtain Mach stem height. This method frequently involved extrapolation of two- or three-point data curves, which would not be expected to be precise.

DISCUSSION OF RESULTS

SHOCK STRENGTH

The effects of roughness on the surface peak overpressure and Mach stem characteristics which have been determined in this investigation are the combined effects of many roughness elements which contribute to the shock-propagation pattern. These results do not indicate the relative contribution of any one, or one group, of roughness elements. Because of the small scale of this investigation, it would not be possible to resolve from the pressure traces or schlieren photographs

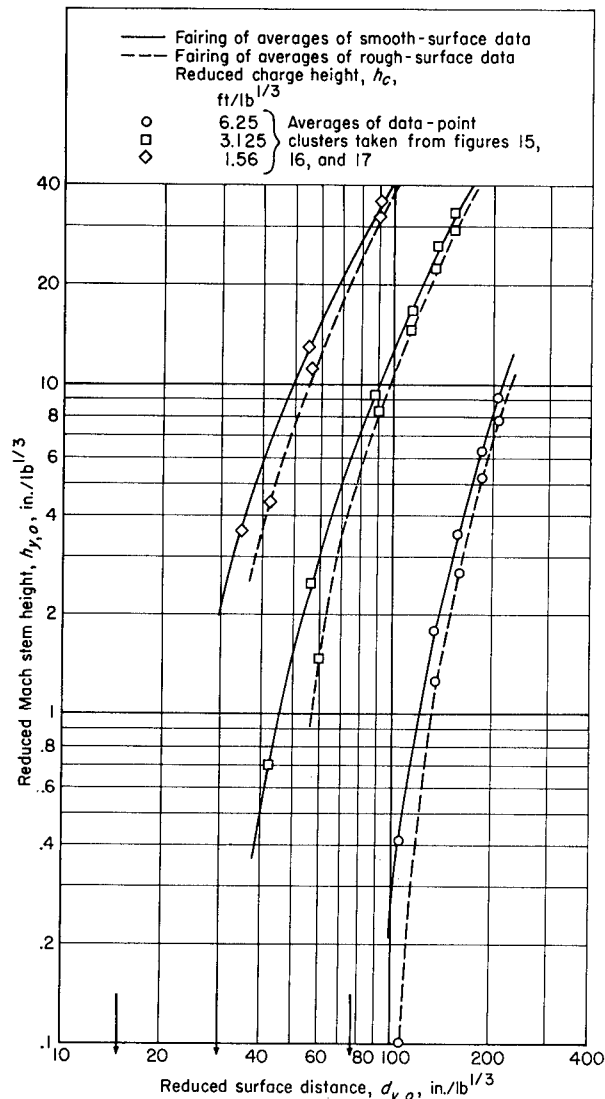


FIGURE 18.—Comparison of Mach stem growth over smooth and rough surfaces at three heights of burst. Arrows represent abscissas for theoretical points of Mach stem formation d_e .

the effects of earlier or later events on the overall pattern. It would seem logical to assume that individual elements or groups of elements do not have a strong effect on the overall shock characteristics in view of the small effect found for many elements. Because of the small scale of the tests and the arrangement of the elements, it is also impossible to detect short-duration irregularities in shock movement (i.e., diffraction effects) such as those that occur locally each time a roughness element is encountered. (See the many small reflected waves in figs. 4(d), 4(e), and 4(f).) The effects of such properties as roughness shape, or

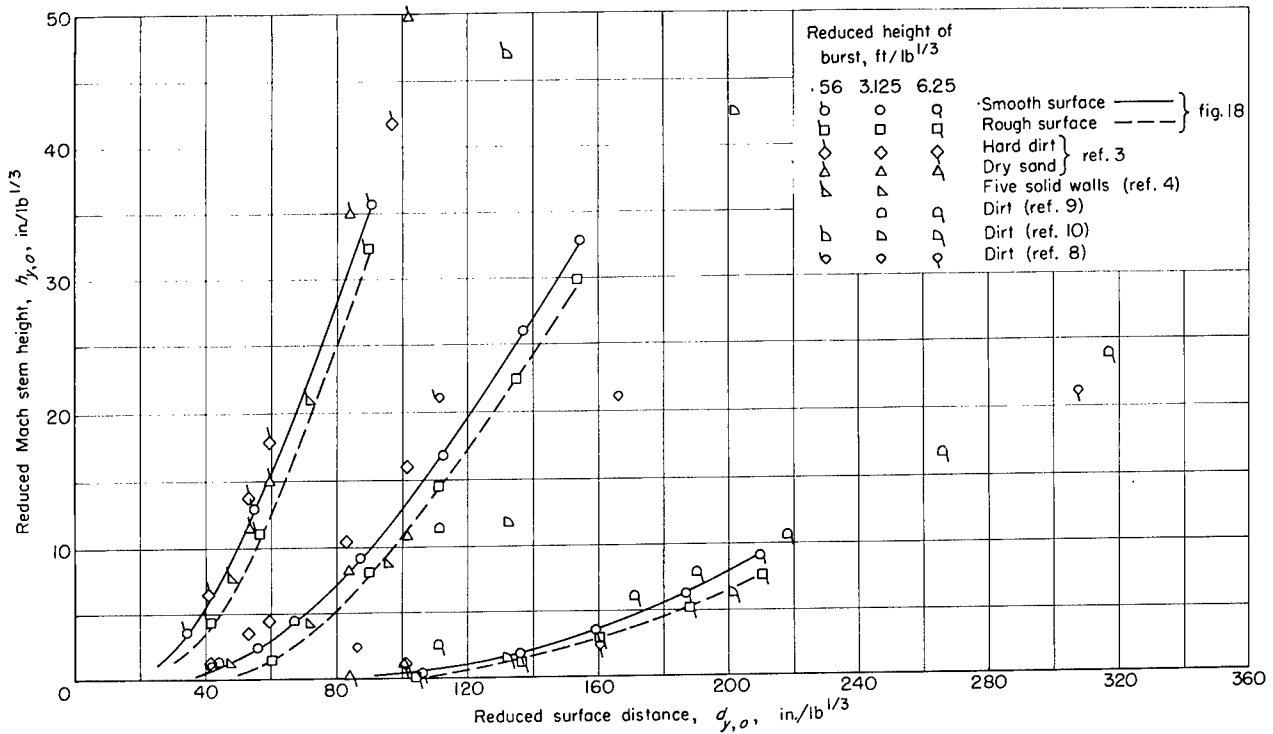


FIGURE 19.—Comparison of Mach stem growth with reference data.

roughness spacing, on the shock-wave strength in the immediate vicinity of the elements cannot, therefore, be concluded.

One important result of surface roughness on shock-wave characteristics is the retardation of air flow near the surface (that is, within a region consisting of a few roughness heights above the surface). This boundary layer in the air flow following the shock as a result of viscous air forces in the region of the roughness results in some momentum loss to the system; however, since the amount of air flow involved in this region is small compared with the total air flow involved in the whole system, the net effect of this momentum loss on the shock-wave strength is seen to be small. This velocity defect near the surface, however, might very well be significant with regard to the drag forces and dynamic characteristics of bodies located in this region since the dynamic pressure would be lowered. Unfortunately, the determination of shock-wave strength does not yield much information concerning these local air-flow velocities. The velocity fields about single bodies located on a smooth surface in spherical-blast-wave flow have been determined in reference 11 by a unique

experimental method and were found to be confined within a region with a radius of a few body heights.

MACH STEM

The measurements of Mach stem height which have been presented herein are believed to represent more precise values than previous methods because these values are obtained from direct observation of the event. Although such small-scale data might be intuitively looked upon with reservations, the free-air shock measurements have shown (see fig. 6) that scaling did not noticeably affect these wave-propagation data. It is true that scaling down of the test layout, such as was done in this investigation, results in air-flow Reynolds numbers which are very much smaller than those obtained in the full-scale test with the result that viscous effects may not be similar. Reference 12 shows, however, that the influence of Reynolds number on wave-diffraction phenomena was small in the case of a sharp-edged body in a shock tube. This information indicates that any changes in flow about the body with Reynolds number had little effect on the incident-shock-wave pattern. Therefore, in view of the small effects

on overall shock strength that are due to an extreme surface roughness, it is doubtful if a Reynolds number effect is herein significant with regard to the Mach stem data. The local air-flow characteristics about the roughness elements might be more noticeably influenced by Reynolds number, however, particularly for rounded or smoothly faired bodies where flow separation is not fixed by the geometry as much as it is fixed for sharp-edged bodies. (See ref. 11.)

The Mach stem results which are plotted in figures 15 to 17 have been examined in the light of a possible geometrical similarity of the triple-point path for different heights of burst. Although there is no theoretical justification for

similarity based on the parameters d_e , h_e , and α_e , in references 3 and 10 the results were plotted in the form of ϕ against $\alpha - \alpha_e$ in which a single curve was considered to be representative of all the data. In figure 20, all the Mach stem data obtained in this investigation have been plotted in the same form as the data in references 3 and 10, and the result can be seen to be still dependent upon the height of burst. The data of references 3 and 10 are also plotted for comparison and show some dependence upon height of burst rather than appear as a random scatter of data about a single curve.

The most similarity of the Mach stem data for various heights of burst was found when the

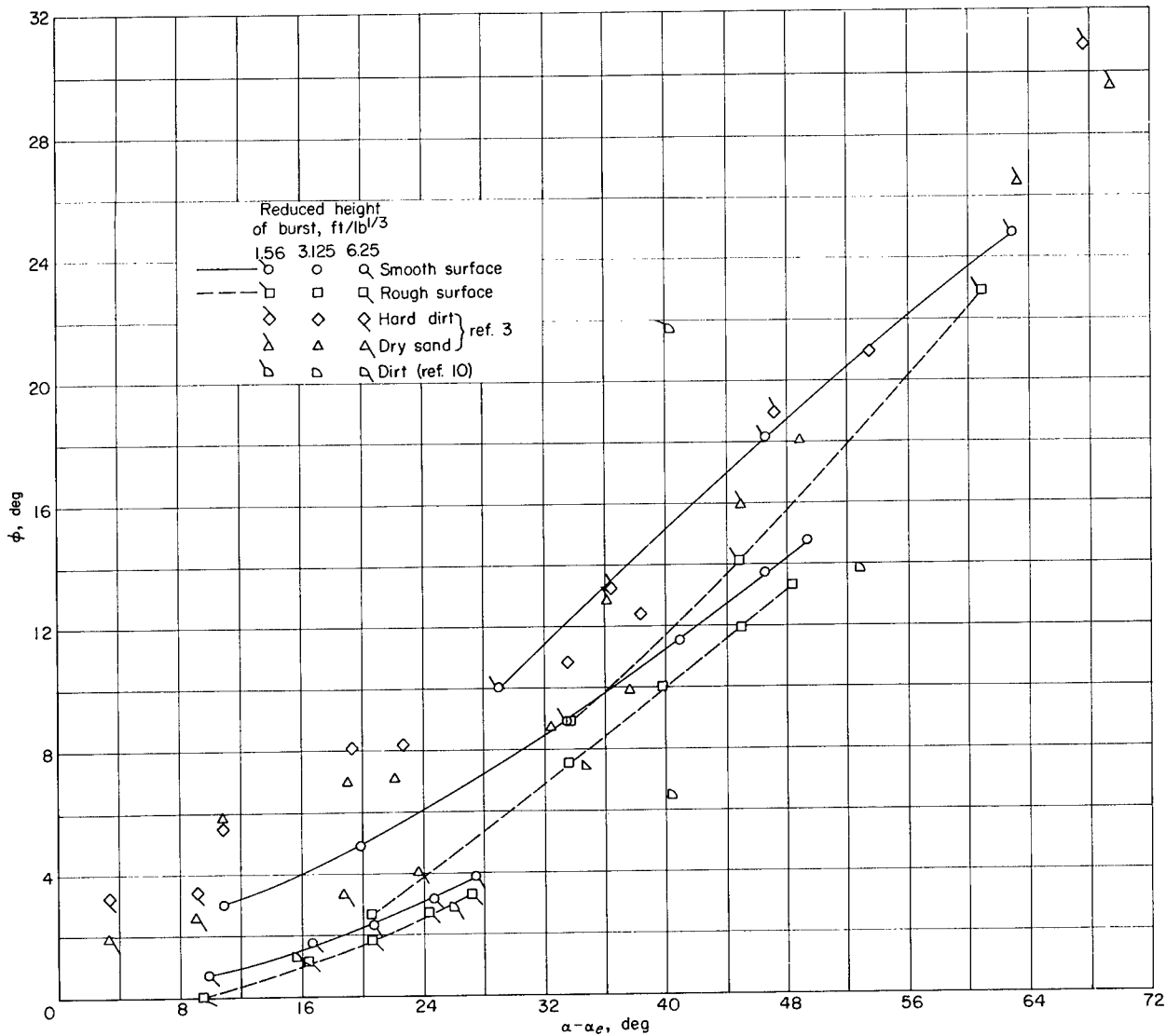


FIGURE 20.—Path of triple point based on height-of-burst similarity parameter in reference 10.

data were plotted in the form shown in figure 21, where $\left(\frac{d_y-d_e}{d_e}\right)_0$ is plotted against the reduced Mach stem height $h_{y,o}$. Although the data have not been reduced to a single curve, there is somewhat less dependence on h_e than appears in figure 20. The data of references 3 and 10 are also shown for comparison in figure 21, and the dependence on height of burst is again seen to be less than that in figure 20.

CONCLUSIONS

Measurements of peak overpressure and Mach stem height have been made for spherical shock waves moving over smooth and rough surfaces at four different charge heights. The data were obtained on a small-scale test layout with 15-gram

pentolite charges and instrumentation capable of directly observing the variation of shock-wave movement with time. The following conclusions may be drawn from examination of the data and comparison with reference data:

1. Good similarity of the relationship between free-air shock peak overpressure and distance with larger scale data was found to exist.
2. The net effect of extreme surface roughness on the relationship of shock peak overpressure at the surface against distance for all heights of burst was to lower the overpressures slightly.
3. The effect of extreme surface roughness on the Mach stem formation was to delay the formation at the greatest charge height (6.25 ft/lb^{1/3}).
4. The effect of extreme surface roughness on the growth of the Mach stem with horizontal

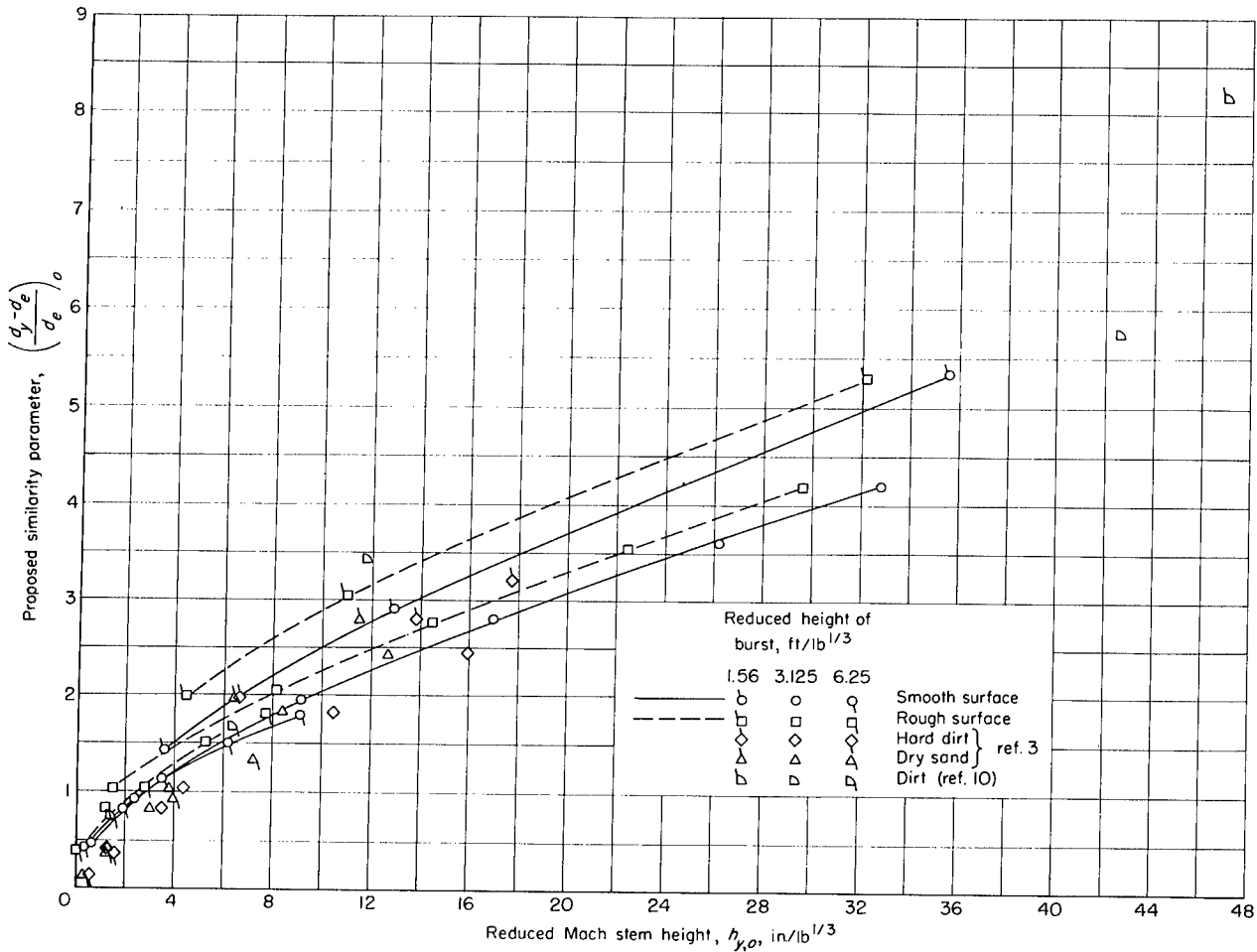


FIGURE 21.—Approximate similarity of path of triple-point rise with height of burst based on $\left(\frac{d_y-d_e}{d_e}\right)_0$.

distance was to lower the Mach stem height at all heights of bursts.

5. The data did not fit a geometrical similarity parameter for the path of the triple point at different heights of burst as suggested by other investigators. A simple similarity parameter was

found which showed only a small influence of burst height on the path of the triple point.

LANGLEY RESEARCH CENTER,
NATIONAL AERONAUTICS AND SPACE ADMINISTRATION,
LANGLEY FIELD, VA., July 30, 1959.

REFERENCES

1. Anon.: The Effects of Atomic Weapons, U.S. Atomic Energy Comm., June 1950, pp. 45-82.
2. Glasstone, Samuel, ed.: The Effects of Nuclear Weapons. U.S. Atomic Energy Comm., June 1957, pp. 73-120.
3. Bryant, E. J., Eberhard, R. A., and Kingery, C. N.: Mach Reflection Over Hard Packed Dirt and Dry Sand. Rep. No. 809, Ballistic Res. Labs., Aberdeen Proving Ground, July 1952.
4. Eberhard, R. A., Stoering, J. P., and Coulter, G.: Effect of Solid Walls on the Mach Region. Rep. No. 759, Ballistic Res. Labs., Aberdeen Proving Ground, May 1951.
5. Huber, Paul W., and McFarland, Donald R.: Boundary-Layer Growth and Shock Attenuation in a Shock Tube With Roughness. NACA TN 3627, 1956.
6. Curtis, Wesley: Free Air Blast Measurements on Spherical Pentolite. Memo. Rep. No. 544, Ballistic Res. Labs., Aberdeen Proving Ground, July 1951.
7. Hartmann, G. K., and Kalavski, P. Z.: The Optimum Height of Burst for High Explosives. NAVORD Rep. 2451, U.S. Naval Ord. Lab. (White Oak, Md.), July 21, 1952.
8. Taub, A. H.: The Effect of Height of Burst on the Blast From Explosives. NDRC Rep. No. A-486 (OSRD Rep. No. 6660), Div. 2, Mar. 1946.
9. Stoner, R. G.: Mach Reflection of Shock Waves From Charges Detonated in Air. Study of Shock Waves (Project OD-03). Vol. 3—Air and Earth Shock, NDRC Monthly Rep. No. AES-3 (OSRD No. 4257), Div. 2, Oct. 25, 1944, pp. 17-37.
10. Halverson, R. R.: The Effect of Air Burst on the Blast From Bombs and Small Charges—II. Analysis of Experimental Results. NDRC Rep. No. A-320 (OSRD Rep. No. 4899), Div. 2, Apr. 6, 1945.
11. McFarland, Donald R.: Investigation of Spherical-Wave-Initiated Flow Fields Around Bodies. NASA MEMO 1-6-59L, 1959.
12. Griffith, W. C., Welmer, D. K., Brickl, D. E., and Bleakney, Walker: The Effect of Reynolds Number on the Diffraction of a Shock Wave. Tech. Rep. II-8 (Contract N6ori-105), Dept. of Phys., Princeton Univ., Feb. 1951.